Nanoscale

PAPER

View Article Online
View Journal | View Issue

Cite this: *Nanoscale*, 2016, **8**, 10113

Solution-based intramolecular singlet fission in cross-conjugated pentacene dimers†

Johannes Zirzlmeier,[a] Rubén Casillas,[a] S. Rajagopala Reddy,[b] Pedro B. Coto,[b] Dan Lehnherr,[c] Erin T. Chernick,[d] Ilias Papadopoulos,[a] Michael Thoss,[b] Rik R. Tykwinski*[d] and Dirk M. Guldi*[a]

Received 25th March 2016,
Accepted 29th March 2016

DOI: 10.1039/c6nr02493a

www.rsc.org/nanoscale

We show unambiguous and compelling evidence by means of pump–probe experiments, which are complemented by calculations using *ab initio* multireference perturbation theory, for intramolecular singlet fission (SF) within two synthetically tailored pentacene dimers with cross-conjugation, namely **XC1** and **XC2**. The two pentacene dimers differ in terms of electronic interactions as evidenced by perturbation of the ground state absorption spectra stemming from stronger through-bond contributions in **XC1** as confirmed by theory. Multiwavelength analysis, on one hand, and global analysis, on the other hand, confirm that the rapid singlet excited state decay and triplet excited state growth relate to SF. SF rate constants and quantum yields increase with solvent polarity. For example, **XC2** reveals triplet quantum yields and rate constants as high as 162 ± 10% and (0.7 ± 0.1) × 10^{12} s^{-1}, respectively, in room temperature solutions.

Introduction

Currently, singlet fission (SF), in which one singlet excited state is converted into two triplet excited states,[1,2] serves as the primary means to overcome the Shockley–Queisser limit.[3–6] A number of energetic and conformational requirements must be satisfied to realize SF. Among these requirements, the most important component is the energy of the singlet excited state, $E(S_1)$, relative to the energy of the triplet excited state, $E(T_1)$, namely $E(S_1) \geq 2(E(T_1))$.[1,2,7,8] Early stage investigations of intermolecular SF focused on crystalline materials.[5,9–15] With respect to SF efficiency, crystal packing, molecular orbital overlap, *etc*. of the chromophores are decisive.[16–18]

SF has been documented for tetra-, penta-, and hexacene in the solid state,[19–24] as well as for tetra- and pentacene in solution.[25–28] In the solid state, tetracene features nearly degenerate singlet excited states and correlated pairs of triplet excited states, *i.e.*, $E(S_1) \approx 2E(T_1)$, rendering the standard enthalpy for intermolecular SF negligible. In contrast, the singlet excited state energy in pristine pentacene in the solid state is more than twice the energy of a correlated pair of two triplet excited states, namely $E(S_1) \geq 2(E(T_1))$. Thus, SF is exoergic and unidirectional for pentacene. In hexacene, SF is linked to the formation of a correlated pair of triplet excited states and phonons.[5,9,23,29–31]

In contrast to SF in the solid state, SF in solution has only recently been discovered for pentacenes, with yields reaching as high as 200%.[26–28] Solution-state SF has also been demonstrated in tetracene dimers, but with a SF yield of only 3%.[25]

It is logical to hypothesize that the relative proximity between neighboring acenes is critical to the process of SF, and the molecular geometry as well as the π–π overlap would be dominant factors for efficient SF.[32–35] One can envision a plethora of acenes that might be synthesized to explore specific aspects of SF in dimeric structures.[36–39] We have recently described the photophysical behavior of a set of three regioisomeric pentacene dimers, linked *via* an ***ortho***-, ***meta***-, and ***para***-phenylene (Fig. 1).[27] The observed triplet quantum yield in these dimers is as high as 156 ± 5%. It is interesting to note that the ***meta***-linked dimer gives the best SF performance, a molecule in which the two pentacenes are not directly conjugated through the intervening phenylene ring, in contrast to either the ***ortho***- or ***para***-linked dimer. In light of the general structure of the ***meta***-dimer, we speculate that moderating the electronic communication between two acene chromophores

[a]*Department of Chemistry and Pharmacy & Interdisciplinary Center for Molecular Materials (ICMM), Engineering of Advanced Materials (EAM), Friedrich-Alexander-Universität Erlangen-Nürnberg (FAU), Egerlandstrasse 3, 91058 Erlangen, Germany. E-mail: dirk.guldi@fau.de*
[b]*Institute for Theoretical Physics & Interdisciplinary Center for Molecular Materials (ICMM), Friedrich-Alexander-Universität Erlangen-Nürnberg (FAU), Staudtstrasse 7/B2, 91058 Erlangen, Germany. E-mail: michael.thoss@fau.de*
[c]*Department of Chemistry, University of Alberta, Edmonton, Alberta T6G 2G2, Canada. E-mail: lehnherr@cornell.edu*
[d]*Department of Chemistry and Pharmacy & Interdisciplinary Center for Molecular Materials (ICMM), Friedrich-Alexander-Universität Erlangen-Nürnberg (FAU), Henkestrasse 42, 91054 Erlangen, Germany. E-mail: rik.tykwinski@fau.de*
†Electronic supplementary information (ESI) available. See DOI: 10.1039/c6nr02493a

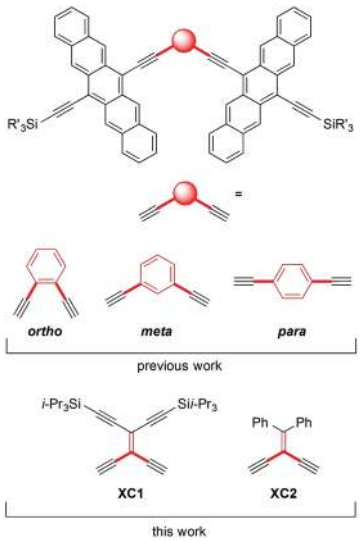

Fig. 1 Phenylene tethered pentacene dimers studied previously[27] and cross-conjugated pentacene dimers investigated in the present work.

might be an important design concept for the optimization of SF. In order to test this hypothesis, dimers based on diethynyl- and tetraethynylethenes (DEE and TEE, respectively) have been designed, in which the two pentacenes communicate in the ground state only *via* cross-conjugation.[40,41] The constrained conjugation of DEEs and TEEs has been used, for example, to form molecular wires,[42–44] switches,[45] and nonlinear optical materials.[46] Furthermore, the contrasting behavior of chromophores linked by ***meta***-phenylene groups *versus* a cross-conjugated skeleton has been a topic of somewhat controversial discussion in organic electronics.[47,48]

Considering the excited states that are involved, their nature, and their electronic coupling, two main mechanisms for SF have been proposed over the years, the direct and the mediated, and the predominance of one or another remains a subject of controversy.[2,7,9,17,32,49–62] In the direct mechanism, the absorbing state transforms into a correlated pair of triplet excited states, also called multiexcitonic (ME) or doubly excited state, which later dissociates into two (non-interacting) T_1 states. In the mediated mechanism, the transformation of the absorbing state into the ME state, which then dissociates into two T_1 states, is facilitated by coupling to higher-lying CT states.[2,55] Recent studies have refined these traditional viewpoints, providing more information about the detailed interplay of the different electronic states involved in the process. In particular, one of the studies postulates that the initial excitation of the molecular system produces a state that is not an eigenstate of the system but a coherent superposition of the (lowest-lying) absorbing state, CT states, and the ME state.[9,17] The latter ultimately splits into two separated T_1 states after decoherence. Finally, a very recent model suggests that the non-interacting T_1 states are directly populated from the absorbing state without the participation of any intermediate electronic state in the process.[62]

In the present contribution, we have designed and examined two novel pentacene dimers **XC1** and **XC2**, that feature a cross-conjugated framework to mediate the electronic coupling between the two pentacene moieties. The cross-conjugated structural modification is expected to be particularly helpful as a means to either enhance or attenuate the through bond electronic couplings between the pentacene chromophores.[41] Furthermore, **XC1** and **XC2** feature rigid structures, with geometries that are similar to that found in ***ortho***-dimer (*vide infra*).

Results and discussion

Synthesis

Cross-conjugated dimers **XC1** and **XC2** were synthesized from the reaction of masked pentacene **1**, which has proven to be a valuable precursor for the stepwise assembly of pentacene derivatives *via* transition metal catalyzed reactions.[27,37,39] Thus, the reaction of **1** with either dibromoolefin **2**[63] or **3**[64] was carried out using a Sonogashira cross-coupling protocol, and the TEE and DEE cores of **4** and **5** were formed in acceptable yields of 63% and 60%, respectively (Scheme 1).

Subsequently, Sn(II)-mediated reductive aromatization afforded **XC1** and **XC2** in 82% and 95% yield, respectively. Dimers **XC1** and **XC2** are stable to air and moisture under

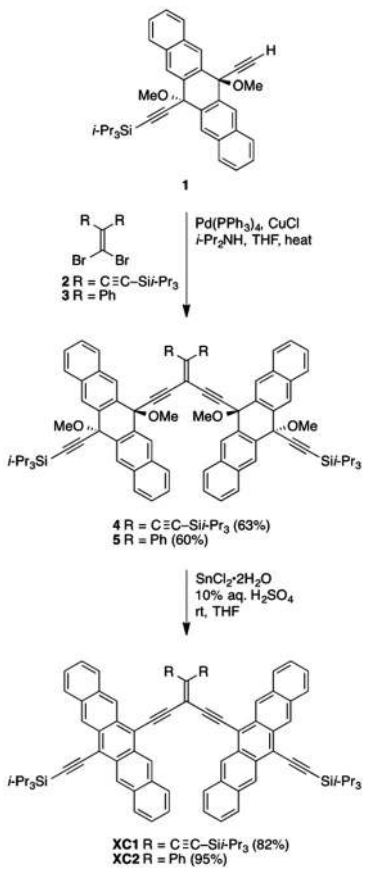

Scheme 1 Synthesis of **XC1** and **XC2**.

normal laboratory conditions, and they have good solubility in typical organic solvents.

A single crystal of **XC2** suitable for X-ray crystallographic analysis was grown from a THF solution layered with MeOH and allowed to evaporate at 4 °C. The solid-state structure emphasizes the proximity of the two pentacenes. Fig. 2 documents that through space interactions are accessible in both the solid and solution states *via* carbon–carbon contacts between the two pentacene units as short as 3.34 Å (in the crystal), a result that agrees well with that found theoretically (3.41 Å, see ESI†).

Singlet and triplet excited state energetics

We turned to absorption and emission spectroscopies combined with electrochemical analyses to establish the singlet and triplet excited state energetics. In terms of ground state features, we note short wavelength absorptions in the region of 350–500 nm and long wavelength absorptions in the 500–775 nm region (Fig. 3). As a result of the rigid structure of **XC1** and **XC2**, both sets of absorptions show distinct vibrational fine structures. The spectroscopically relevant long wavelength absorptions are at 681 nm (**XC1**) and 683 nm (**XC2**). In concentration dependent experiments, which obey the Lambert–Beer law for dilute solutions, the following extinction coefficients were determined in benzonitrile: 28 800 M^{-1} cm^{-1} (**XC1**) and 48 900 M^{-1} cm^{-1} (**XC2**). It is notable that the values for **XC1** and **XC2** are less or exactly twice that of TIPS pentacene **7** (Fig. 4), respectively. A likely rationale infers stronger electronic communications between the two pentacenes in **XC1** relative to **XC2**.

In terms of excited state features, exciting into the long wavelength absorptions leads to fluorescence maxima at 691 and 688 nm and fluorescence quantum yields of 0.03 ± 0.01% and 0.12 ± 0.04% for **XC1** and **XC2**, respectively, in benzonitrile. Notably, these features are all linked to the singlet excited state with energies of 1.81 eV. Finally, no appreciable triplet excited state phosphorescence is observed for **XC1** or **XC2** in either solutions at room temperature or in frozen media experiments upon excitation in the long wavelength absorption region.

To complement absorption and fluorescence studies, squarewave voltammetric analyses of **XC1** and **XC2** have been carried out in benzonitrile solutions containing 0.1 M $TBAPF_6$ as supporting electrolyte. From the one electron oxidations at +0.44 and +0.35 V, as well as the one electron reductions at −1.27 and −1.39 V for **XC1** and **XC2** (*versus* Fc/Fc^+), respectively, highest occupied molecular orbital/lowest unoccupied molecular orbital gaps of 1.71 and 1.74 eV are calculated, which are in sound agreement with the absorption/fluorescence assays.

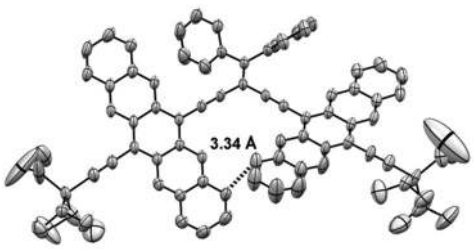

Fig. 2 X-ray crystallographic structure of **XC2** illustrating the spatial arrangement and proximity of the two pentacene units in the dimer. THF solvent molecules and hydrogen atoms have been omitted for clarity.

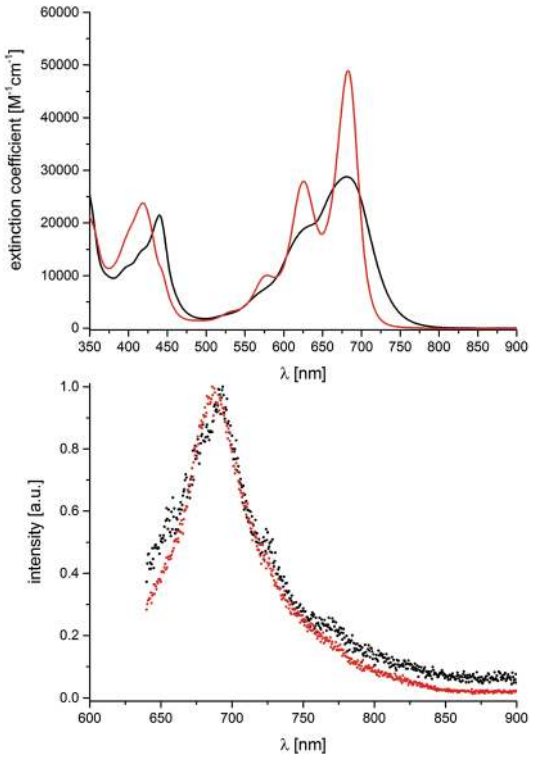

Fig. 3 Top: Room temperature absorption spectra of **XC1** (black line) and **XC2** (red line) in benzonitrile. Bottom: Normalized fluorescence spectra of **XC1** (black dots) and **XC2** (red dots) in benzonitrile solutions following photoexcitation at 625 nm with an optical density of 0.05. The corresponding fluorescence quantum yields in benzonitrile are 0.03 ± 0.01% for **XC1** and 0.12 ± 0.04% for **XC2** (measured relative to a zinc phthalocyanine used as a reference compound[65]).

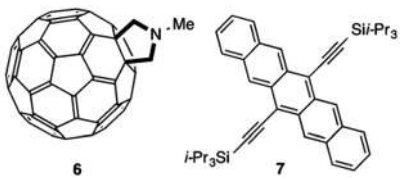

Fig. 4 Molecular structures of C_{60} derivative **6** and TIPS pentacene **7**.

TIPS pentacene

First, we examined **7** in 2-methyltetrahydrofuran (Me-THF, 3.0×10^{-4} M) with excitation at 656 nm to stimulate population of only vibrational states of the first singlet excited state manifold (Fig. 5). Additionally, the photon flux has been adjusted to 6.6×10^9 photons per pulse to excite, on average, 10% or less of **7** in its ground state in order to rule out multiple excitations.

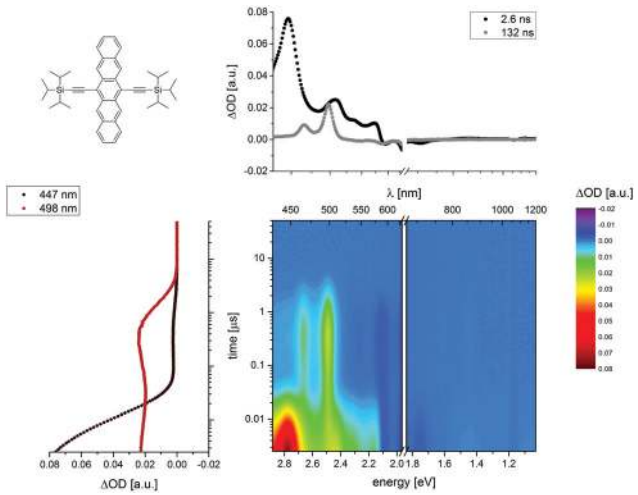

Fig. 5 Upper left: Chemical structure of TIPS pentacene **7**. Upper right: Differential absorption spectra (visible and near-infrared) of the spectra shown in the lower right with time delays of 2.6 ns (black) and 132 ns (gray). Lower left: Time absorption profiles of the spectra shown in the lower right at 447 nm (black), and 498 nm (red) illustrating the dynamics of the singlet excited state formation followed by the singlet to triplet transformation in the form of intersystem crossing, and triplet decay. Lower right: Differential absorption changes (visible and near-infrared) obtained upon femtosecond pump probe experiments (656 nm) of **7** (3.0×10^{-4} M) in argon-saturated Me-THF at room temperature with several time delays between 0 and 50 μs.

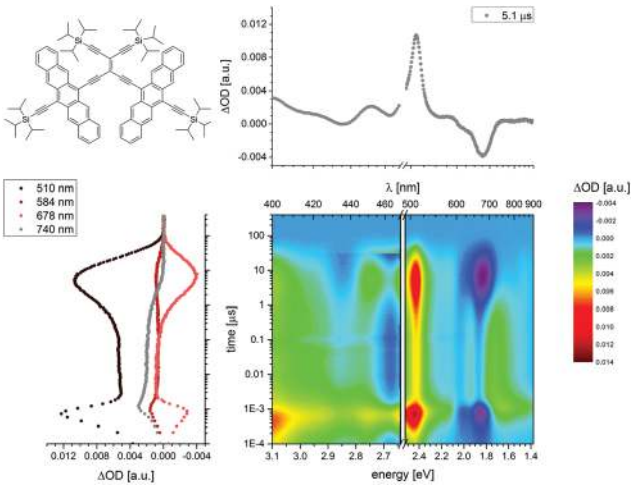

Fig. 6 Upper left: Chemical structure of **XC1**. Upper right: Differential absorption spectrum (visible and near-infrared) of the spectra shown in the lower right with a time delay of 5.1 μs representing the triplet excited state of **XC1**. Lower left: Time absorption profiles of the spectra shown in the lower right at 510 nm (black), 584 nm (red), 678 nm (orange), and 740 nm (gray) illustrating the dynamics of the **6** singlet excited state formation followed by the intersystem crossing to the corresponding **6** triplet excited state and transduction of triplet excited state energy to **XC1**. Lower right: Differential absorption changes (visible and near-infrared) obtained upon femtosecond pump probe experiments (480 nm) of **6** (8.0×10^{-5} M) and **XC1** (1.0×10^{-4} M) in argon-saturated toluene at room temperature with several time delays between 0 and 400 μs.

For photoexcited **7**, the major deactivation pathway includes a 12.3 ± 0.1 ns intersystem crossing, through which the singlet excited state transforms into the corresponding triplet manifold. Once formed, the triplet excited state deactivates with 24.0 ± 0.5 μs to reinstate the singlet ground state of **7**. As far as the singlet excited state characteristics are concerned, maxima at 447, 508, 538, 572, 845, and 1400 nm are noted, as well as minima at 595 and 641 nm. An additional feature at 710 nm is observed, which corresponds to stimulated emission. Triplet excited state characteristics include maxima at 465 and 498 nm and minima at 546, 587, and 641 nm. Owing to a moderate triplet quantum yield of only 16% for **7** the resulting characteristics turn out to be extremely weak.

Triplet–triplet sensitization

To investigate the triplet excited states characteristics *via* an inefficient intersystem crossing – *vide supra* – we turned to intermolecular, that is, diffusion or activation controlled, triplet–triplet sensitization experiments using the well-studied C_{60} derivative **6** as a photosensitizer to examine the triplet excited state characteristics of **7** as well as of **XC1** and **XC2** (Fig. 4, 6 and S9–S17†). Incentives for the use of **6** are an excitation wavelength independent triplet quantum yield of unity, a triplet excited state energy 1.5 eV higher than that of **7**, **XC1**, and **XC2**, a triplet excited state molar extinction coefficient of 16 000 M^{-1} cm^{-1} at its transient maximum at 695 nm, and a lack of chemical reactions with pentacene derivatives in the applied concentration range.[66] Excitation of **6** at 480 nm (8.0×10^{-5} M) resulted in differential absorption changes on the nanosecond/microsecond time scale featuring a 695 nm maximum and a 840 nm shoulder. These originate from a 1.5 ns intersystem crossing between the corresponding singlet and triplet excited manifolds. In the absence of **7**, **XC1**, **XC2**, and molecular oxygen, these features decay within 33.0 ± 1.0 μs due to triplet–triplet and triplet-ground state annihilations. Addition of **7**, **XC1**, or **XC2** in the concentration range from 10^{-5} to 10^{-4} M affords nearly diffusion-controlled deactivations of the triplet excited state of **6** with rate constants on the order of 2.5×10^9 M^{-1} s^{-1}.[67,68] Simultaneously with such a faster decay newly developing transient features are noted including a maximum at 510 nm and a minimum at 678 nm for **XC1** as well as a maximum at 508 nm and minima at 622 and 679 nm for **XC2**. Here, the excited state minima are precise mirror images of the ground state absorption maxima. Notable is also the close resemblance with the features seen for **7** and several other pentacence dimers,[27] from which we conclude a transduction of triplet excited state energy to **XC1** and **XC2**. The lifetimes of the triplet excited states of **XC1** and **XC2** are bimolecular in nature. From the corresponding rate constants, namely $(1.1 \pm 0.1) \times 10^8$ and $(0.7 \pm 0.1) \times 10^8$ M^{-1} s^{-1} for **XC1** and **XC2**, respectively, we deduce activation limited triplet excited state decays including triplet–triplet annihilation as a major component and collision induced triplet–ground state annihilation as a minor component.

With the triplet excited state molar extinction coefficients of **6** at hand, we calculated the triplet excited state extinction coefficients at the 508 nm maximum, the 622 nm minimum, and the 679 nm minimum at each concentration of **XC2**, as well as at the 510 nm maximum and the 678 nm minimum of **XC1**. By plotting the extinction coefficients as a function of concentration, we noticed a saturation behavior towards the high concentration regime. At an extrapolation to 5×10^{-4} M the triplet–triplet sensitization is quantitative relative to the initially photoexcited **6**. Of importance is the fact that the molar extinction coefficients of 21 200 and 52 800 M^{-1} cm^{-1} for **XC2** at the 622 nm minimum and the 679 nm minimum, respectively, are in sound agreement with the ground state molar extinction coefficients of 30 800 and 57 900 M^{-1} cm^{-1} at 620 and 678 nm, respectively. Likewise the value of 28 700 M^{-1} cm^{-1} for **XC1** at its 678 nm minimum matches that seen at 675 nm in the ground state absorption. From the aforementioned we infer quantitative bleaching of the ground state for **XC1** or **XC2** and, in turn, triplet excited states, in which both pentacenes are excited. Considering pseudo first order conditions, namely a laser intensity that is equivalent to approximately 10^{-7} M triplet excited state of **6** and 5.0×10^{-5} M of **XC1** or **XC2**, we postulate that the triplet excited state molar extinction coefficients are only half of the extrapolated values, that is, 45 200, 10 600 and 26 400 M^{-1} cm^{-1} at the 508 nm maximum, the 622 nm minimum, and the 679 nm minimum, respectively. In fact, with this assumption they are identical to what has been seen for **7**, which features molar extinction coefficients about half of that of **XC2**.

To substantiate our postulate we performed actinometry using pristine C_{60}.[69] Here, we used solutions of pristine C_{60} with four different concentrations and solutions of either **7**, **XC1**, or **XC2**, each of them with exactly the same absorptions at the 387 nm excitation wavelength, and pumped them with the same laser power. In Fig. S18,† the intensities of the C_{60} singlet excited state markers, on one hand, and the **7**, **XC1**, and **XC2** singlet as well as triplet excited state markers, on the other hand, are plotted as a function of absorption. This dependence documents the linear dependence of each excited marker within the range of absorptions. Correlating the respective slopes for pristine C_{60} with those for **7**, **XC1**, or **XC2** enable the determination of the molar extinction coefficients for **7**, **XC1**, and **XC2** at, for example, time delays of 1.5 ps. To this end, we determined singlet excited state molar extinction coefficients for **XC2** of 14 400 M^{-1} cm^{-1} at the 622 nm minimum and of 24 100 M^{-1} cm^{-1} at the 677 nm minimum. For **XC1**, the corresponding singlet excited state molar extinction coefficient is 20 200 M^{-1} cm^{-1} at 679 nm. All of these values relate to half of the ground state extinction coefficients/ground state bleaching and suggest singlet excited states, in which only a single pentacene is photoexcited. The latter assumption is in sound agreement with the low laser flux of 6.6×10^{9} photons per pulse. Additional support was provided by the fact that the 647 nm value of 15 000 M^{-1} cm^{-1} for **7** correlates quantitatively with the ground state extinction coefficient/ground state bleaching. In case that **7**, **XC1**, and **XC2** show quantitative intersystem crossing, that is, affording triplet quantum yields of 100%, the triplet excited state molar extinction coefficients at 647, 679, and 677 nm, respectively, should match those of the singlet excited states.

Singlet fission in XC1 and XC2

For **XC2** in benzonitrile, the singlet excited state features are discernable as a 455 nm maximum and a broad band in the NIR as well as minima at 627 and 687 nm directly upon photoexcitation at 656 nm (Fig. 7). In contrast to that observed for **7**, where a slow intersystem crossing dominates the initial 20 ns, the singlet excited state features of **XC2** are replaced within 15 ps by characteristics that match those seen in the triplet–triplet sensitization experiments (Fig. S17†). In particular, these are maxima at 486, 517, 853, and 976 nm and minima at 628 and 685 nm. From multiwavelength analyses, which afforded strictly unimolecular, intramolecular dynamics in the range from 1×10^{-5} to 1×10^{-4} M of **XC2**, we conclude that these features correspond to the rapidly decaying singlet excited state ($(0.7 \pm 0.1) \times 10^{12}$ s^{-1}) and the simultaneously grow of the triplet excited state markers. Please note that there is a slight blue shift, from 687 to 685 nm, as a consequence of this transformation. A closer look at delay times up to 2000 ps, however, reveals the metastability of the newly formed triplet excited state. Considering, on one hand, that the experimental conditions preclude multiple excitations of **XC2** and, on the other hand, that triplet–triplet annihilation contributes most strongly to the triplet excited state decay we tested the

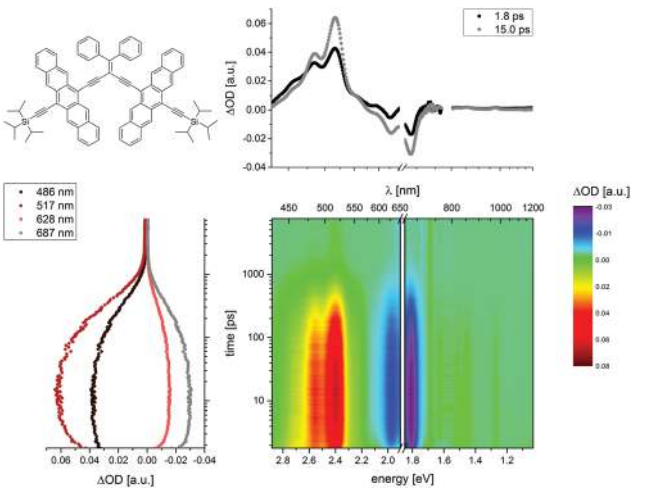

Fig. 7 Upper left: Chemical structure of **XC2**. Upper right: Differential absorption spectra (visible and near-infrared) of the spectra shown in the lower right with time delays of 1.8 ps (black) and 15.0 ps (gray). Lower left: Time absorption profiles of the spectra shown in the lower right at 486 nm (black), 517 nm (red), 628 nm (orange), and 687 nm (gray) illustrating the dynamics of the singlet excited state formation followed by the singlet to triplet transformation in the form of singlet fission and triplet–triplet annihilation. Lower right: Differential absorption changes (visible and near-infrared) obtained upon femtosecond pump probe experiments (656 nm) of **XC2** (5.0×10^{-5} M) in argon-saturated benzonitrile at room temperature with several time delays between 0 and 7500 ps.

impact of different concentrations in the range from 1×10^{-5} to 1×10^{-4} M. Regardless of the concentration, we note only unimolecular and invariant dynamics with a rate constant of $(2.54 \pm 0.08) \times 10^{9}$ s^{-1}. As such, we hypothesize unimolecular triplet–triplet annihilations, which requires that two triplets are localized within **XC2** and this is only feasible by SF – *vide infra*. Spectroscopic corroboration for two photoexcited pentacenes came from a 2–3 nm blue-shift not only relative to the singlet excited state bleaching but also relative to the triplet excited state bleaching seen in direct excitation and triplet–triplet sensitization experiments, respectively. The product of the triplet–triplet annihilations is the singlet ground state of **XC2** *via* radiationless relaxation,[70] and independent on concentration or laser power. But, a spectroscopically invisible excited state cannot be ruled out. As a complement to multiwavelength analyses, we performed global analyses with the Glotaran software package (Fig. 9).[71] The results, as they were obtained from the global fitting, are a qualitative and quantitative match to those gathered in the multiwavelength approach for **XC2** and **XC1**. For example, the singlet excited state in **XC2** transforms sequentially into the triplet excited state and ground state within 0.7 ± 0.1 and 445 ± 20 ps, respectively.

Very similar observations are made for **XC1** in benzonitrile (Fig. 8 and 9), in terms of differential absorption changes and kinetics *versus* **XC2**. In particular, the singlet excited state for **XC1** converts with similar decay and growth kinetics of (0.65 ± 0.1) × 10^{12} s^{-1} *via* SF into a metastable triplet excited state. In THF and toluene the corresponding kinetics tend to be as slow as $(0.63 \pm 0.1) \times 10^{12}$ and $(0.50 \pm 0.1) \times 10^{12}$ s^{-1}. Analyses of the long wavelength minima reveals a blue-shift of 2–3 nm when comparing the singlet and triplet excited state spectra. Similar to **XC2**, the metastability observed for **XC1** is seen in the form of unimolecular, intramolecular triplet–triplet annihilations ($(2.08 \pm 0.07) \times 10^{9}$ s^{-1}). The latter results in fast and quantitative ground state recovery on a time scale of less than 3000 ps. Resembling **XC2**, the two steps, namely SF and the decay of the correspondingly formed triplet excited state, are clearly deconvoluted. If at all, the different cross conjugation in **XC2** results in slightly faster triplet excited state formation and slightly faster triplet excited state decay relative to **XC1**, but the differences are small. The absorption spectra – *vide supra* – point possibly to stronger electronic coupling in **XC1**, which is likely derived from through-bond interactions. As such, we hypothesize that solution SF seems more favorable in the latter scenario.

To corroborate SF as the mechanism for singlet to triplet conversion we have used three different approaches, that is, the sensitization method, the bleaching method, and the actinometry method, to determine the triplet quantum yields. In the first approach, **6** is used as an external reference to derive the transient extinction coefficients. Firstly, we have revisited the triplet–triplet sensitization experiments, whose differential absorption spectra in the high concentration regime, where the triplet energy transfer efficiency is close to unity, enable derivation of triplet molar extinction coefficients for **XC2** of 45 200, 10 600 and 26 400 M^{-1} cm^{-1} at the 508 nm maximum, the 622 nm minimum, and the 679 nm minimum, respectively. Next, we have determined the singlet molar extinction coefficients with the help of conventional femtosecond transient absorption measurements. **XC2**, for example, features only very weak ground state absorption at 456 nm in benzonitrile, and, as such, we take the amplitude of the differential absorptions at 455 nm after 1 ps and relate it entirely to the singlet excited state concentration formed upon excitation. Finally, the differential absorption changes of 0.0242 a.u. at 455 nm and 0.0679 a.u. at 518 nm are converted into concentrations of the singlet excited state of 4.64×10^{-6} M and of the triplet excited state of 7.51×10^{-6} M. This ultimately converts to a triplet quantum yield of 162 ± 10% for **XC2**.

Independent confirmation of the triplet quantum yield comes from the second approach (bleaching method), in which no external reference is used to calculate the transient extinction coefficients of the singlet and triplet excited state. In this case, the amplitudes of the ground state bleaching in benzonitrile at 687 nm (−0.0245 a.u) and 685 nm (−0.0314 a.u.) are used to calculate the transient concentrations as 4.64×10^{-6} and 5.96×10^{-6} M for the singlet and the triplet excited state, respectively. This affords a triplet quantum yield of 128 ± 5% for **XC2**. The high triplet quantum yield along with its ultrafast formation provide strong evidence that the triplet excited state for **XC2** forms by intramolecular SF between the two pentacenes. Moreover, higher quantum yields in more polarizable solvents –

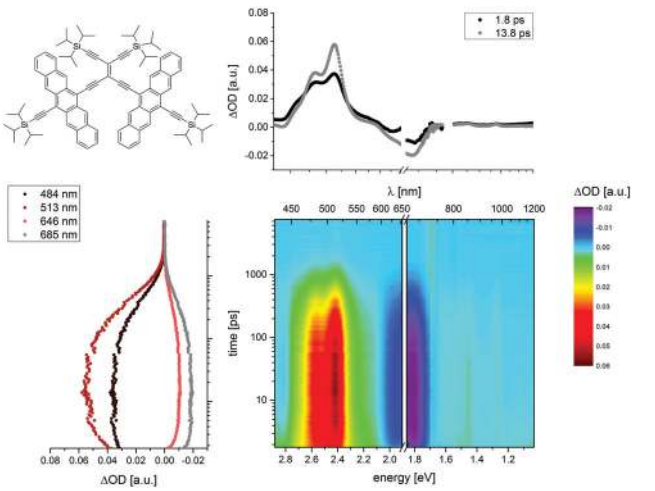

Fig. 8 Upper left: Chemical structure of **XC1**. Upper right: Differential absorption spectra (visible and near-infrared) of the spectra shown in the lower right with time delays of 1.8 ps (black) and 13.8 ps (gray). Lower left: Time absorption profiles of the spectra shown in the lower right at 484 nm (black), 513 nm (red), 646 nm (orange), and 685 nm (gray) illustrating the dynamics of the singlet excited state formation followed by the singlet to triplet transformation in the form of singlet fission and triplet–triplet annihilation. Lower right: Differential absorption changes (visible and near-infrared) obtained upon femtosecond pump probe experiments (656 nm) of **XC1** (5.0×10^{-5} M) in argon-saturated benzonitrile at room temperature with several time delays between 0 and 7500 ps.

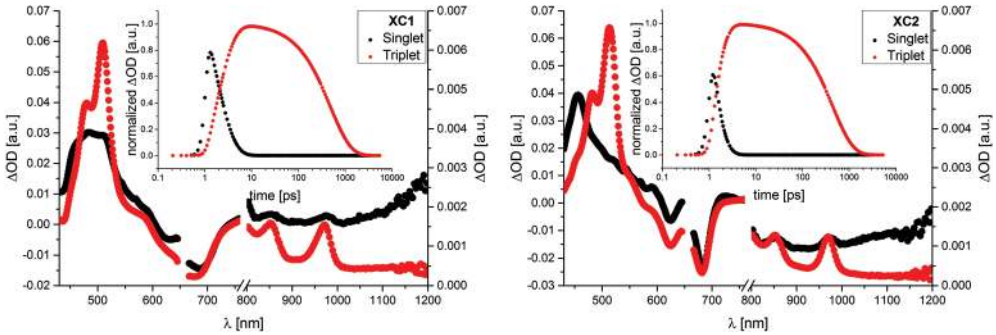

Fig. 9 Deconvoluted transient absorption spectra of the singlet (black) and the triplet excited state (red) of **XC1** and **XC2** as obtained by global analysis (visible and near-infrared). Inset: Evolution of the population of the singlet (black) and the triplet excited state (red).

mean values of 128 ± 10% in toluene *versus* 162 ± 10% in benzonitrile – corroborate the charge transfer nature of the mediating step. Analogously, the triplet quantum yields for **XC1** are derived as 127 ± 10% with an external reference and 124 ± 5% without an external reference in benzonitrile. In toluene, the corresponding yields for **XC1** are lower with values of 119 ± 10% and 114 ± 5%, respectively (Table 1).[72] In a third approach we used the results from the actinometry experiments to calculate the triplet quantum yields. Correlating the slopes for the respective singlet and triplet excited state features enable the determination of triplet quantum yields of 111 ± 5% for **XC1** and 107 ± 5% for **XC2** in toluene, in good agreement with the results obtained by means of the first and second approach.

Theory

To further solidify the experimental results, we have investigated the electronic states of relevance for SF using multireference perturbation theory methods (see ESI† for details). The calculated vertical excitation energies, dipole moments, oscillator strengths, and character of the relevant adiabatic states are summarized in Table 2. For **XC1** and **XC2**, the ME state is the lowest-lying singlet excited state (see Table 2 and ESI†). Furthermore, the vertical excitation energies of the lowest-lying absorbing S_2 state of **XC1** (1.88 eV) and **XC2** (1.90 eV) agree well with the experimental data. Both **XC1** and **XC2** exhibit CT states (S_4 and S_5) with moderate dipole moments that are relatively high in energy (~0.5–0.6 eV) compared to the S_2 state.

Table 1 Triplet excited state quantum yields ($\Phi_{Triplet}$) for **XC1** and **XC2** calculated *via* the sensitization method, the bleaching method, and the actinometry

		Sensitization method	Bleaching method	Actinometry
		Triplet quantum yield [%]		
XC1	Toluene	119	114	111
	THF	131	121	—
	Benzonitrile	127	124	—
XC2	Toluene	128	109	107
	THF	144	113	—
	Benzonitrile	162	128	—

To shed light on the SF mechanism, we have determined the diabatic electronic states and their couplings employing Truhlar's four-fold-way diabatization procedure (see ESI†).[73,74] We report in the following the results obtained for **XC1** and **XC2**. Following previous works,[2,18,60] the diabatic states are classified as the singlet ground state $|S_0S_0\rangle$, the correlated triplet pair (or ME) state $|T_1T_1\rangle$, the locally excited (in one pentacene chromophore) singlet states $|S_1S_0\rangle$ and $|S_0S_1\rangle$ and the charge transfer states $|CA\rangle$ and $|AC\rangle$. In the latter, one of the two pentacenes is formally a radical cation (C), while the other is a radical anion (A). For **XC1** and **XC2**, the diabatic coupling matrices are presented in Table 3. As Table 3 documents, **XC1** and **XC2** each exhibit a moderate electronic coupling between the locally excited states ($|S_1S_0\rangle$ and $|S_0S_1\rangle$) and $|T_1T_1\rangle$. Specifically, $|S_1S_0\rangle$ and $|S_0S_1\rangle$ couple to $|T_1T_1\rangle$ with a strength of 9 and −12 meV, respectively, in **XC1**. In **XC2**, the corresponding values are −1 and 2 meV. In contrast, the electronic coupling between $|S_1S_0\rangle$ or $|S_0S_1\rangle$, and the charge transfer states $|CA\rangle$ and $|AC\rangle$ range from 30 to 140 meV. As such, this is nearly an order of magnitude larger than that between the locally excited and the correlated triplet pair state $|T_1T_1\rangle$ (Table 3). $|T_1T_1\rangle$ also couples to the $|CA\rangle$ and $|AC\rangle$ states with 10–60 meV in **XC1** and 23–27 meV in **XC2**.

To dissect contributions from either the direct or the mediated SF mechanism and the role of CT states, we estimated the magnitude of the effective coupling, V_{eff}, of the lowest lying absorbing singlet state $|S_1S_0\rangle$ to $|T_1T_1\rangle$ (similar for $|S_0S_1\rangle$ to $|T_1T_1\rangle$) as:[55,75]

$$V_{eff} \approx V_{S_1S_0,T_1T_1} - 2\frac{V_{S_1S_0,CA}V_{CA,T_1T_1} + V_{S_1S_0,AC}V_{AC,T_1T_1}}{[E(CT) - E(T_1T_1)] + [E(CT) - E(S_1S_0)]} \quad (1)$$

where $E(i)$ are the energies of the corresponding diabatic states, E(CT) is the mean of E(CA) and E(AC), and $V_{i,j}$ are the couplings between the states i and j. The first term in eqn (1) denotes the direct coupling and the second term the indirect coupling mediated by the CT states. The results in Table 4 indicate that in both **XC1** and **XC2** the direct coupling of $|S_1S_0\rangle$ to $|T_1T_1\rangle$ is significantly smaller than the indirect coupling *via* CT states. The differences between both types of coupling are smaller in the case of **XC2** relative to **XC1**. For the second bright state $|S_0S_1\rangle$, which is quasi-degenerate to $|S_1S_0\rangle$,

Table 2 Vertical excitation energy (ΔE in eV),[a] modulus of the dipole moment (μ, D),[b] oscillator strength (f),[b] and character for the lowest lying singlet excited states (char.)[c] of **XC1** and **XC2**

	XC1				**XC2**			
State	ΔE	μ	f	Char.	ΔE	μ	f	Char.
S_1	1.82	2.31	<0.001	ME	1.84	0.06	<0.001	ME
S_2	1.88	4.43	0.880	LE	1.90	1.74	0.770	LE
S_3	1.94	3.39	0.610	LE	1.95	1.74	0.640	LE
S_4	2.31	8.23	0.004	CT	2.36	8.31	0.005	CT
S_5	2.40	8.79	0.002	CT	2.40	8.33	0.001	CT

[a] Calculated at the XMCQDPT/DZV level of theory. [b] Calculated at the CASSCF level of theory. [c] Character of excited state: ME = multiexcitonic state, LE = excited states that correlate with the plus and minus combinations of locally excited states of both pentacene monomers, CT = charge transfer states.

Table 3 Energies and coupling matrix elements (meV) of the low-lying diabatic electronic states of **XC1** (top) and **XC2** (bottom) calculated at the XMCQDPT/DZV level of theory

XC1	$\|S_0S_0\rangle$	$\|T_1T_1\rangle$	$\|S_1S_0\rangle$	$\|S_0S_1\rangle$	$\|CA\rangle$	$\|AC\rangle$
$\|S_0S_0\rangle$	0	10	261	105	81	18
$\|T_1T_1\rangle$	10	1779	9	−12	61	11
$\|S_1S_0\rangle$	261	9	1863	−29	141	71
$\|S_0S_1\rangle$	105	−12	−29	1885	−31	34
$\|CA\rangle$	81	61	141	−31	2217	21
$\|AC\rangle$	18	11	71	34	21	2323
XC2	$\|S_0S_0\rangle$	$\|T_1T_1\rangle$	$\|S_1S_0\rangle$	$\|S_0S_1\rangle$	$\|CA\rangle$	$\|AC\rangle$
$\|S_0S_0\rangle$	0	−13	−119	139	−140	−118
$\|T_1T_1\rangle$	−13	1806	−1	2	−27	23
$\|S_1S_0\rangle$	−119	−1	2009	−94	−136	−72
$\|S_0S_1\rangle$	139	2	−94	2025	138	87
$\|CA\rangle$	−140	−27	−136	138	2172	−130
$\|AC\rangle$	−118	23	−72	87	−130	2282

Table 4 Direct, indirect, and total coupling (meV) of the lowest lying absorbing singlet states $|S_1S_0\rangle$ and $|S_0S_1\rangle$ to $|T_1T_1\rangle$ for **XC1** and **XC2**, calculated at the XMQCDPT/DZV level of theory using Truhlar's four-fold-way diabatization method

System	State	Direct	Indirect	Total
XC1	$\|S_1S_0\rangle$	9.39	−23.69	−14.30
	$\|S_0S_1\rangle$	−12.09	3.94	−8.15
XC2	$\|S_1S_0\rangle$	−0.83	−7.62	−8.45
	$\|S_0S_1\rangle$	1.78	6.72	8.50

XC1 exhibits an effective coupling smaller than that found for $|S_1S_0\rangle$ and where the major contribution stems from the direct coupling of $|S_0S_1\rangle$ to $|T_1T_1\rangle$. On the other hand, **XC2** shows an effective coupling between $|S_1S_0\rangle$ and $|T_1T_1\rangle$ where the major contribution corresponds to the indirect coupling *via* CT states. Considering that the CT states are higher in energy than the absorbing states we postulate that SF is likely to proceed predominantly *via* a superexchange-like mechanism in both molecular systems, although in the case of **XC1** we expect a more significant contribution of the direct mechanism to the overall process than in **XC2** (see Table 4). This is further corroborated by the experimentally found dependence of the triplet quantum yield on the polarizability of the solvents employed. The results in Table 4 also indicate that the coupling is somewhat larger in **XC1** compared to **XC2**, which may explain the stronger broadening of the absorption spectrum of **XC1** (see Fig. 3).

Conclusions

We have designed cross-conjugated pentacene dimers, **XC1** and **XC2**, to fine-tune the electronic coupling element between the two pentacenes and to gain control over intramolecular SF in room temperature solutions. To this end, **XC1** features slightly stronger electronic coupling, governed by through-bond interactions, than **XC2**. Kinetic and spectroscopic analyses were based on applications of multiwavelength analysis, on one hand, and global analysis using the program Glotaran, on the other hand. Both led to identical results and corroborate that the cross-conjugated tethers maintain the electronic couplings lending, however, to slightly higher triplet quantum yields for **XC2** than for **XC1**. As a matter of fact, the highest triplet quantum yield observed is 162 ± 10%.

Our synthetic, spectroscopic, and computational efforts highlight the importance of establishing the right balance between triplet excited state formation/singlet excited state deactivation and triplet excited state decay towards the optimization of SF. An outstanding question remains the loss mechanism(s) from the singlet state in our dimers, and ongoing work in our laboratories focuses on realizing SF quantum yields close to unity through further controlling intramolecular interactions in synthetically designed dimers.

Experimental section

The synthesis of **XC1** and **XC2**, materials, general methods, and computational details are described in the ESI†.

For the photophysical characterization (see ESI†), the samples were placed in fluorometric cuvettes with different pathways and, when necessary, purged with argon. Steady-state UV-vis absorption spectra were acquired at room temperature (RT) using a Perkin Elmer Lambda 2 spectrometer. Steady-

state fluorescence spectra were carried out at a FluoroMax3 spectrometer from Horiba in the visible detection range (RT) and at a FluoroLog3 spectrometer from Horiba in the near infrared. Femtosecond (fs) transient absorption experiments were carried out with an amplified Ti:Sapphire CPA-2110 fs laser system (ClarkMXR: output 775 nm, 1 kHz, 150 fs pulse width) using transient absorption pump/probe detection systems (Helios and Eos, Ultrafast Systems).

The theoretical characterization was based on the following methods. The ground state equilibrium geometries of **XC1** and **XC2** were optimized using density functional theory (DFT),[76] employing the B3LYP correlation-exchange functional and the def2-TZVP basis set.[77,78] Dispersion interactions were taken into account using Grimme's empirical dispersion correction.[78] Vertical excitation energies were calculated using the extended multi-configurational quasi-degenerate perturbation theory (XMCQDPT)[79] method and a double-ζ basis set,[80] employing state average (SA) complete active space self-consistent field (CASSCF)[81,82] wave-functions as reference and an intruder state avoidance shift of 0.02 au.[83] The active space employed in the SA-CASSCF calculations comprised four electrons in four orbitals (HOMO and LUMO per pentacene unit) and six roots with equal weights were used. Dipole moments and oscillator strengths were calculated at the SA-CASSCF level. Diabatic states were built using Truhlar's four-fold-way of diabatization method implemented in GAMESS.[73,74,84] All calculations were carried out using the electronic structure packages TURBOMOLE[85] and GAMESS.[86]

Acknowledgements

We thank Dr R. McDonald for solving the crystal structure of **XC2**. Generous allocation of computing time at the computing centers Erlangen (Regionales Rechenzentrum Erlangen), Munich (Leibniz-Rechenzentrum der Bayerischen Akademie der Wissenschaften in München), and Jülich (Jülich Supercomputing Centre) is gratefully acknowledged. Funding is gratefully acknowledged from the Emerging Fields initiative "Singlet Fission" supported by Friedrich-Alexander-Universität Erlangen-Nürnberg, the German Research Foundation (DFG), as well as the Cluster of Excellence Engineering of Advanced Materials and "Solar Technologies Go Hybrid" – an initiative of the Bavarian State Ministry for Science, Research, and Art.

Notes and references

1 J. C. Johnson, A. J. Nozik and J. Michl, *Acc. Chem. Res.*, 2013, **46**, 1290–1299.
2 M. B. Smith and J. Michl, *Chem. Rev.*, 2010, **110**, 6891–6936.
3 W. Shockley and H. J. Queisser, *J. Appl. Phys.*, 1961, **32**, 510–519.
4 L. Yang, M. Tabachnyk, S. L. Bayliss, M. L. Böhm, K. Broch, N. C. Greenham, R. H. Friend and B. Ehrler, *Nano Lett.*, 2015, **15**, 354–358.
5 W. L. Chan, M. Ligges and X. Y. Zhu, *Nat. Chem.*, 2012, **4**, 840–845.
6 D. N. Congreve, J. Lee, N. J. Thompson, E. Hontz, S. R. Yost, P. D. Reusswig, M. E. Bahlke, S. Reineke, T. Van Voorhis and M. A. Baldo, *Science*, 2013, **340**, 334–337.
7 T. C. Berkelbach, M. S. Hybertsen and D. R. Reichman, *J. Chem. Phys.*, 2013, **138**, 114102.
8 G. B. Piland, J. J. Burdett, R. J. Dillon and C. J. Bardeen, *J. Phys. Chem. Lett.*, 2014, **5**, 2312–2319.
9 W. L. Chan, T. C. Berkelbach, M. R. Provorse, N. R. Monahan, J. R. Tritsch, M. S. Hybertsen, D. R. Reichman, J. Gao and X. Y. Zhu, *Acc. Chem. Res.*, 2013, **46**, 1321–1329.
10 J. J. Burdett and C. J. Bardeen, *Acc. Chem. Res.*, 2013, **46**, 1312–1320.
11 C. E. Swenberg and W. T. Stacy, *Chem. Phys. Lett.*, 1968, **2**, 327–328.
12 T. C. Berkelbach, M. S. Hybertsen and D. R. Reichman, *J. Chem. Phys.*, 2014, **141**, 074705.
13 W. G. Albrecht, M. E. Michel-Beyerle and V. Yakhot, *J. Lumin.*, 1979, **20**, 147–149.
14 A. Rao, M. W. B. Wilson, S. Albert-Seifried, R. Di Pietro and R. H. Friend, *Phys. Rev. B: Condens. Matter*, 2011, **84**, 195411.
15 W. L. Chan, M. Ligges, A. Jailaubekov, L. Kaake, L. Miaja-Avila and X. Y. Zhu, *Science*, 2011, **334**, 1541–1545.
16 C. J. Bardeen, *Annu. Rev. Phys. Chem.*, 2014, **65**, 127–148.
17 N. Monahan and X.-Y. Zhu, *Annu. Rev. Phys. Chem.*, 2015, **66**, 601–618.
18 M. B. Smith and J. Michl, *Annu. Rev. Phys. Chem.*, 2013, **64**, 361–386.
19 R. E. Merrifield, P. Avakian and R. P. Groff, *Chem. Phys. Lett.*, 1969, **3**, 155–157.
20 J. J. Burdett, A. M. Müller, D. Gosztola and C. J. Bardeen, *J. Chem. Phys.*, 2010, **133**, 144506.
21 C. Jundt, G. Klein, B. Sipp, J. Le Moigne, M. Joucla and A. A. Villaeys, *Chem. Phys. Lett.*, 1995, **241**, 84–88.
22 M. Rei Vilar, M. Heyman and M. Schott, *Chem. Phys. Lett.*, 1983, **94**, 522–526.
23 E. Busby, T. C. Berkelbach, B. Kumar, A. Chernikov, Y. Zhong, H. Hlaing, X. Y. Zhu, T. F. Heinz, M. S. Hybertsen, M. Y. Sfeir, D. R. Reichman, C. Nuckolls and O. Yaffe, *J. Am. Chem. Soc.*, 2014, **136**, 10654–10660.
24 J. Lee, M. J. Bruzek, N. J. Thompson, M. Y. Sfeir, J. E. Anthony and M. A. Baldo, *Adv. Mater.*, 2013, **25**, 1445–1448.
25 A. M. Müller, Y. S. Avlasevich, W. W. Schoeller, K. Müllen and C. J. Bardeen, *J. Am. Chem. Soc.*, 2007, **129**, 14240–14250.
26 B. J. Walker, A. J. Musser, D. Beljonne and R. H. Friend, *Nat. Chem.*, 2013, **5**, 1019–1024.
27 J. Zirzlmeier, D. Lehnherr, P. B. Coto, E. T. Chernick, R. Casillas, B. S. Basel, M. Thoss, R. R. Tykwinski and D. M. Guldi, *Proc. Natl. Acad. Sci. U. S. A.*, 2015, **112**, 5325–5330.

28 S. N. Sanders, E. Kumarasamy, A. B. Pun, M. T. Trinh, B. Choi, J. Xia, E. J. Taffet, J. Z. Low, J. R. Miller, X. Roy, X. Y. Zhu, M. L. Steigerwald, M. Y. Sfeir and L. M. Campos, *J. Am. Chem. Soc.*, 2015, **137**, 8965–8972.
29 J. E. Anthony, *Chem. Rev.*, 2006, **106**, 5028–5048.
30 M. W. Wilson, A. Rao, J. Clark, R. S. Kumar, D. Brida, G. Cerullo and R. H. Friend, *J. Am. Chem. Soc.*, 2011, **133**, 11830–11833.
31 K. von Burg and I. Zschokke-Gränacher, *J. Chem. Phys.*, 1979, **70**, 3807–3811.
32 P. M. Zimmerman, Z. Zhang and C. B. Musgrave, *Nat. Chem.*, 2010, **2**, 648–652.
33 S. R. Yost, J. Lee, M. W. B. Wilson, T. Wu, D. P. McMahon, R. R. Parkhurst, N. J. Thompson, D. N. Congreve, A. Rao, K. Johnson, M. Y. Sfeir, M. G. Bawendi, T. M. Swager, R. H. Friend, M. A. Baldo and T. Van Voorhis, *Nat. Chem.*, 2014, **6**, 492–497.
34 L. Wang, Y. Olivier, O. V. Prezhdo and D. Beljonne, *J. Phys. Chem. Lett.*, 2014, **5**, 3345–3353.
35 K. Aryanpour, A. Shukla and S. Mazumdar, *J. Phys. Chem. C*, 2015, **119**, 6966–6979.
36 D. Lehnherr, J. Gao, F. A. Hegmann and R. R. Tykwinski, *Org. Lett.*, 2008, **10**, 4779–4782.
37 D. Lehnherr, A. H. Murray, R. McDonald and R. R. Tykwinski, *Angew. Chem., Int. Ed.*, 2010, **49**, 6190–6194, (*Angew. Chem.*, 2010, **122**, 6326–6330).
38 D. Lehnherr and R. R. Tykwinski, *Aust. J. Chem.*, 2011, **64**, 919–929.
39 A. R. Waterloo, S. Kunakom, F. Hampel and R. R. Tykwinski, *Macromol. Chem. Phys.*, 2012, **213**, 1020–1032.
40 M. Gholami and R. R. Tykwinski, *Chem. Rev.*, 2006, **106**, 4997–5027.
41 P. A. Limacher and H. P. Luthi, *Wiley Interdiscip. Rev.: Comput. Mol. Sci.*, 2011, **1**, 477–486.
42 G. C. Solomon, D. Q. Andrews, R. H. Goldsmith, T. Hansen, M. R. Wasielewski, R. P. Van Duyne and M. A. Ratner, *J. Am. Chem. Soc.*, 2008, **130**, 17301–17308.
43 G. C. Solomon, D. Q. Andrews, R. P. Van Duyne and M. A. Ratner, *J. Am. Chem. Soc.*, 2008, **130**, 7788–7789.
44 G. C. Solomon, C. Herrmann, T. Hansen, V. Mujica and M. A. Ratner, *Nat. Chem.*, 2010, **2**, 223–228.
45 D. Q. Andrews, G. C. Solomon, R. P. Van Duyne and M. A. Ratner, *J. Am. Chem. Soc.*, 2008, **130**, 17309–17319.
46 C. Bosshard, R. Spreiter, P. Günter, R. R. Tykwinski, M. Schreiber and F. Diederich, *Adv. Mater.*, 1996, **8**, 231–234.
47 D. Q. Andrews, G. C. Solomon, R. H. Goldsmith, T. Hansen, M. R. Wasielewski, R. P. V. Duyne and M. A. Ratner, *J. Phys. Chem. C*, 2008, **112**, 16991–16998.
48 K. G. L. Pedersen, A. Borges, P. Hedegård, G. C. Solomon and M. Strange, *J. Phys. Chem. C*, 2015, **119**, 26919–26924.
49 E. C. Greyson, J. Vura-Weis, J. Michl and M. A. Ratner, *J. Phys. Chem. B*, 2010, **114**, 14168–14177.
50 P. M. Zimmerman, F. Bell, D. Casanova and M. Head-Gordon, *J. Am. Chem. Soc.*, 2011, **133**, 19944–19952.
51 R. W. A. Havenith, H. D. de Gier and R. Broer, *Mol. Phys.*, 2012, **110**, 2445–2454.
52 P. E. Teichen and J. D. Eaves, *J. Phys. Chem. B*, 2012, **116**, 11473–11481.
53 P. M. Zimmerman, C. B. Musgrave and M. Head-Gordon, *Acc. Chem. Res.*, 2013, **34**, 1339–1347.
54 N. Renaud, P. A. Sherratt and M. A. Ratner, *J. Phys. Chem. Lett.*, 2013, **4**, 1065–1069.
55 T. C. Berkelbach, M. S. Hybertsen and D. R. Reichman, *J. Chem. Phys.*, 2013, **138**, 114103.
56 D. Beljonne, H. Yamagata, J. L. Brédas, F. C. Spano and Y. Olivier, *Phys. Rev. Lett.*, 2013, **110**, 226402.
57 X. Feng, A. V. Luzanov and A. I. Krylov, *J. Phys. Chem. Lett.*, 2013, **4**, 3845–3852.
58 A. V. Akimov and O. V. Prezhdo, *J. Am. Chem. Soc.*, 2014, **136**, 1599–1608.
59 A. B. Kolomeisky, X. Feng and A. I. Krylov, *J. Phys. Chem. C*, 2014, **118**, 5188–5195.
60 T. Zeng, R. Hoffmann and N. Ananth, *J. Am. Chem. Soc.*, 2014, **136**, 5755–5764.
61 D. Casanova, *J. Chem. Theory Comput.*, 2014, **10**, 324–334.
62 A. J. Musser, M. Maiuri, D. Brida, G. Cerullo, R. H. Friend and J. Clark, *J. Am. Chem. Soc.*, 2015, **137**, 5130–5139.
63 T. Lange, J.-D. van Loon, R. R. Tykwinski, M. Schreiber and F. Diederich, *Synthesis*, 1996, 537–550.
64 A. R. Suárez and M. R. Mazzieri, *J. Org. Chem.*, 1987, **52**, 1145–1147.
65 P. S. Vincett, E. M. Voigt and K. E. Rieckhoff, *J. Chem. Phys.*, 1971, **55**, 4131–4140.
66 M. Maggini and D. M. Guldi, in *Organic, Physical and Materials Photochemistry*, ed. V. Ramamurthy and K. S. Schanze, Marcel Dekker, New York, 2000, vol. 6, pp. 149–196.
67 The rate constants for the diffusion controlled transduction of triplet excited state energy are $(2.4 \pm 0.1) \times 10^9$ and $(2.6 \pm 0.3) \times 10^9$ M^{-1} s^{-1} for **XC1** and **XC2**, respectively.
68 Details about **7** are reported in ref. 27.
69 D. M. Guldi and M. Prato, *Acc. Chem. Res.*, 2000, **33**, 695–703.
70 N. V. Korovina, S. Das, Z. Nett, X. Feng, J. Joy, R. Haiges, A. I. Krylov, S. E. Bradforth and M. E. Thompson, *J. Am. Chem. Soc.*, 2016, **138**, 617–627.
71 J. J. Snellenburg, S. P. Laptenok, R. Seger, K. M. Mullen and I. H. M. van Stokkum, *J. Stat. Soft.*, 2012, **49**, 1–22.
72 Using the bleaching at around 625 nm to calculate the triplet quantum yields with the bleaching method, results in a similar trend. For **XC1**, the quantum yields are derived as 139 ± 5% in toluene and 150 ± 5% in benzonitrile, for **XC2**, the corresponding values are 139 ± 5% and 180 ± 5%, respectively.
73 H. Nakamura and D. G. Truhlar, *J. Chem. Phys.*, 2001, **115**, 10353–10372.
74 H. Nakamura and D. G. Truhlar, *J. Chem. Phys.*, 2002, **117**, 5576–5593.

75 A. Nitzan, *Chemical Dynamics in Condensed Phases: Relaxation, Transfer, and Reactions in Condensed Molecular Systems*, Oxford University Press, New York, 2014.
76 O. Treutler and R. Ahlrichs, *J. Chem. Phys.*, 1995, **102**, 346–354.
77 F. Weigend and R. Ahlrichs, *Phys. Chem. Chem. Phys.*, 2005, **7**, 3297–3305.
78 F. Weigend, *Phys. Chem. Chem. Phys.*, 2006, **8**, 1057–1065.
79 A. A. Granovsky, *J. Chem. Phys.*, 2011, **134**, 214113.
80 T. H. Dunning Jr. and P. J. Hay, in *Methods of Electronic Structure Theory*, ed. H. F. Schaefer III, Plenum Press, New York, 1997, vol. 3, pp. 1–28.
81 B. R. Brooks and H. F. Schaefer, *J. Chem. Phys.*, 1979, **70**, 5092–5106.
82 B. R. Brooks, W. D. Laidig, P. Saxe, N. C. Handy and H. F. Schaefer III, *Phys. Scr.*, 1980, **21**, 312–322.
83 H. A. Witek, Y.-K. Choe, J. P. Finley and K. Hirao, *J. Comput. Chem.*, 2002, **23**, 957–965.
84 M. W. Schmidt, K. K. Baldridge, J. A. Boatz, S. T. Elbert, M. S. Gordon, J. H. Jensen, S. Koseki, N. Matsunaga, K. A. Nguyen, S. Su, T. L. Windus, M. Dupuis and J. A. Montgomery, *J. Comput. Chem.*, 1993, **14**, 1347–1363.
85 TURBOMOLE V6.6 2014, a development of University of Karlsruhe and Forschungszentrum Karlsruhe GmbH, 1989–2007, TURBOMOLE GmbH, since 2007, available from http://www.turbomole.com.
86 M. S. Gordon and M. W. Schmidt, in *Theory and Applications of Computational Chemistry: the first forty years*, ed. C. E. Dykstra, G. Frenking, K. S. Kim and G. E. Scuseria, Elsevier, Amsterdam, 2005, pp. 1167–1189.